Computers and Geotechnics 77 (2016) 1–10

Contents lists available at ScienceDirect

Computers and Geotechnics

journal homepage: www.elsevier.com/locate/compgeo

Research Paper

Analytical solution for infiltration and deep percolation of rainwater into a monolithic cover subjected to different patterns of rainfall

T.L.T. Zhan, Q.W. Qiu *, W.J. Xu

MOE Key Laboratory of Soft Soils and Geoenvironmental Engineering, Zhejiang University, Hangzhou 310058, China

ARTICLE INFO

Article history:
Received 29 October 2015
Received in revised form 16 February 2016
Accepted 21 March 2016

Keywords:
Different patterns of rainfall
Infiltration
Monolithic cover
Deep percolation
Analytical solution

ABSTRACT

Monolithic cover is increasingly considered for use at landfills of solid wastes in arid and semi-arid areas. The evaluation of the deep percolation of rainwater through the monolithic cover is required for the cover design. An analytical solution is developed in this study for evaluating the infiltration and deep percolation of rainwater into a monolithic cover, subject to different patterns of rainfall events. The analytical solution is derived from the simplified one-dimensional governing equation of unsaturated flow for an infinitely long monolithic cover by taking the exponential forms of the soil–water characteristic curve and the hydraulic conductivity curve into account. A unit gradient boundary (UG) is considered at the bottom boundary of the monolithic cover. The patterns of rainfall considered include uniform type (U), advanced type (A1 and A2), central-peaked type (C), and delayed type (D1 and D2). The delayed percolation after the completion of a rainfall event can be captured by the analytical solution. Numerical simulation is conducted to compare the results with the analytical solution and to demonstrate that the analytical solution is acceptable for describing a silty soil, which is commonly used as the material for a monolithic cover. The analytical solution is used to investigate the influence of the rainfall pattern on the infiltration process and the occurrence of deep percolation. The analytical solution is used to evaluate the total percolation of a monolithic cover subjected to a sequence of non-continuous rainfall events within a wet season. The evaluation accounts for the influence of the initial water storage in the cover on the percolation by using the antecedent rainfall method proposed by Crozier and Eyles in 1980. A case study is performed to demonstrate the evaluation approach by using the water balance monitoring data of a model test on a silty soil cover reported in the literature. The case study indicated that the total percolation from the analytical solution is 34% greater than the measurement, which was on the conservative side for practical application.

1. Introduction

As a form of earthen final cover, the monolithic cover is increasingly considered for use at some landfills in arid and semi-arid regions. Unlike conventional covers (e.g., compacted clay layers, geomembranes, and geosynthetic clay liners) that use materials with low hydraulic permeability to minimize the downward migration of rainwater from the cover to the waste (i.e., deep percolation), a monolithic cover uses a single layer of fine-grained soil to retain water until it is either transpired through vegetation or evaporated from the soil surface, so that the production of the percolation is minimized [1,2]. Compared to the conventional covers, the monolithic cover is expected to be less costly to construct and maintain [3]. Laboratory and field experiments have been conducted to evaluate the percolations of monolithic covers in different climate areas [4–6]. The research results show that the monolithic covers are effective in some arid and semi-arid areas [6–8]. In addition, numerical simulations have been conducted using many codes (e.g., UNSAT-H, VADOSE/W and HYDRUS) to evaluate the deep percolation of rainwater through monolithic covers [5,9–11]. In these simulations, the upper boundary was set as an atmospheric boundary condition consisting of evaporation or infiltration, the bottom boundary was often set as a unit gradient boundary (UG) or a seepage face boundary (SF), and the initial water content distribution was set as uniform or non-uniform, according to the actual situation. Experimental and numerical approaches have been widely used to evaluate the deep percolation of rainwater through the monolithic covers. However,

* Corresponding author.
E-mail addresses: zhanlt@zju.edu.cn (T.L.T. Zhan), qiuqingwen105@163.com (Q.W. Qiu), wenjiexu84@gmail.com (W.J. Xu).

http://dx.doi.org/10.1016/j.compgeo.2016.03.008
0266-352X/

such numerical studies are time consuming, and such experiments are costly. The analytical method requires some assumptions to derive closed-form solutions. If the assumptions are reasonable, then the analytical solution becomes a simple and practical tool for calculating the deep percolation of rainwater through monolithic covers [12].

To date, some analytical solutions for rainfall infiltration into horizontal or sloping ground have been studied by many researchers [12–17]. In 1991, Srivastava and Yeh [14] derived analytical solutions for simulating one-dimensional rainfall infiltration into homogeneous and two-layered soils using Laplace transformation. In 2010 and 2012, Zhan et al. [12,13] developed analytical solutions for simulating two-dimensional rainfall infiltration into infinite homogeneous soil and two-layered soils slopes. In 2012, Huang and Wu [15] presented analytical solutions to one-dimensional horizontal and vertical water infiltration in saturated/unsaturated soils. In 2009 and 2012, Wu et al. [16,17] developed analytical solutions for one-dimensional coupled seepage and deformation in homogeneous and two-layer unsaturated soils. However, the bottom boundary conditions used in the above analytical solutions were all the fixed pore water pressure boundary, which differs from the real conditions at the bottom of monolithic covers. The unit gradient boundary (UG) or the seepage face boundary (SF) is commonly used for the numerical computation of deep percolation through monolithic covers. In addition, the upper boundary condition used in the above analytical solutions was generally constant flow flux, which cannot be used to simulate non-uniformly distributed rainfall.

An analytical solution is proposed in this paper for describing rainfall infiltration into a monolithic cover and for calculating its percolation. The analytical solution is able to take six patterns of rainfall into account. The soil–water characteristic curve and hydraulic conductivity curve used in the analytical solution are expressed by exponential functions. A numerical simulation was conducted to verify the analytical solution and to determine the conditions under which the analytical solution is acceptable. The analytical solution was used to study the influence of the six patterns of rainfall on the infiltration and percolation in the monolithic covers. The analytical solution was further applied to evaluate the total percolation of a monolithic cover being subjected to a sequence of non-continuous rainfall events within a wet season. A case study was performed to demonstrate the evaluation approach by using the water balance monitoring data of a model test on a silty soil cover reported in the literature.

2. Infiltration model of the monolithic cover

The schematic diagram of a monolithic cover is shown in Fig. 1. The Cartesian rectangular space coordinates, x and z, are used, with x as a positive value in the horizontal downslope direction and z as a positive value in the upward vertical direction. Another set of Cartesian coordinates are used as the rotated coordinates, namely, x_* and z_*, as defined in Fig. 1. To obtain an analytical solution that can describe rainfall infiltration into the monolithic cover and calculate its percolation, the following five assumptions are made:

(1) The soil of the monolithic cover is homogeneous and does not exhibit a volume change during the wetting and drying process.
(2) The sloping length of the monolithic cover is assumed to be infinite, and the equipotential lines of pore water pressure are parallel to the surface of the slope [12,13]. Thus, the rainfall infiltration into the monolithic cover can be simplified as a one-dimensional problem.
(3) The pore air pressure in the soil, which remains constant and is equal to the atmospheric pressure, does not influence the water migration.
(4) The change of soil temperature has no influence on the water migration.
(5) The hysteresis associated with wetting/drying process is not considered in this paper.

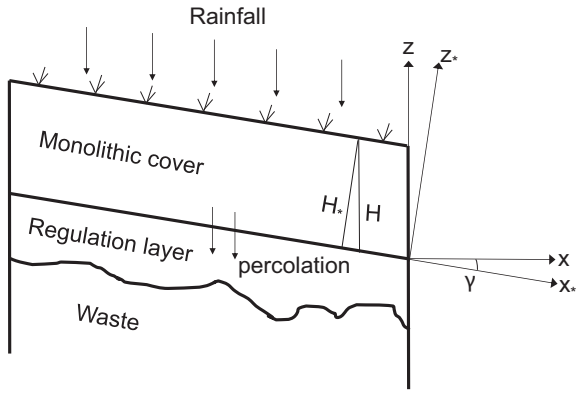

Fig. 1. Schematic diagram of a monolithic cover.

According to the above assumptions, the two-dimensional unsaturated flow of the infinitely long monolithic cover can be simplified and expressed by a one-dimensional governing equation, as shown in Eq. (1). Its detailed derived process and description can be found in the previous literatures [12,13].

$$\frac{\partial}{\partial z_*}\left(k\frac{\partial \psi}{\partial z_*}\right)+\frac{\partial k}{\partial z_*}\cos\gamma=\frac{\partial \theta}{\partial t} \tag{1}$$

where k is the unsaturated hydraulic conductivity, ψ is the pore-water pressure head, γ is the slope angle of the monolithic cover, θ is the volumetric water content, and t is the time.

Eq. (1) is non-linear. To obtain its analytical solution, exponential functional forms are assumed to represent the hydraulic conductivity function and the soil–water characteristic curve (SWCC), as shown in Eqs. (2) and (3) [15,16].

$$k=\begin{cases} k_s e^{\alpha(\psi+\psi_{ae})} & \psi \leqslant -\psi_{ae} \\ k_s & \psi > -\psi_{ae} \end{cases} \tag{2}$$

$$\theta=\begin{cases} \theta_r+(\theta_s-\theta_r)e^{\alpha(\psi+\psi_{ae})} & \psi \leqslant -\psi_{ae} \\ \theta_s & \psi > -\psi_{ae} \end{cases} \tag{3}$$

where k_s is the saturated hydraulic conductivity of the soil used for the monolithic cover, θ_r is the residual moisture content, θ_s is the saturated moisture content, α is a parameter representing the rate of reduction in hydraulic conductivity or moisture content as ψ becomes more negative, and ψ_{ae} is the air-entry value.

With these two exponential functions, Eq. (1) can be transformed to the following linear equations:

$$\frac{\partial^2 k}{\partial z_*^2}+\alpha\cos\gamma\frac{\partial k}{\partial z_*}=\frac{\alpha(\theta_s-\theta_r)}{k_s}\frac{\partial k}{\partial t} \tag{4}$$

The rainfall intensity is measured vertically and must be converted to a component perpendicular to the ground surface (i.e., decreased by the cosine of the slope angle) [18]. Therefore, the upper boundary condition of the monolithic cover can be written as

$$\left(k\cos\gamma+k\frac{\partial \psi}{\partial z_*}\right)\Big|_{z_*=H_*}=q\cos\gamma \qquad t>0 \tag{5}$$

where H_* is the thickness of the monolithic cover, as shown in Fig. 1 and q is the rainfall intensity that can completely infiltrate into the

monolithic cover without considering surface runoff, and it can be constant or vary with time.

Based on a review of the previous numerical simulation studies, the unit gradient boundary (UG) and seepage face boundary (SF) were often used as the bottom boundary. For the UG, the percolation at the bottom is forced to occur continuously under the gravity driven condition at a rate corresponding to the unsaturated hydraulic conductivity. In contrast, the SF permits the percolation to occur only when a saturated condition occurs at the boundary. When the saturation condition occurs, percolation occurs at a rate equal to the saturated hydraulic conductivity at the boundary. Compared to the SF, the UG has been more widely used because it provides a more conservative estimate of deep percolation [8]. Therefore, the bottom boundary in this paper is set as the UG, as shown in Eq. (6).

$$\frac{\partial \psi}{\partial z_*}\Big|_{z_*=0} = 0 \qquad t > 0 \tag{6}$$

The initial condition for the analytical solution is set as uniform volumetric water content distribution, which is expressed using a uniform unsaturated hydraulic conductivity distribution, as shown in the following equation:

$$k = k_0 \qquad 0 \leqslant z_* \leqslant H_*, t = 0 \tag{7}$$

For simplicity, the following dimensionless parameters are defined:

$$\begin{cases} k' = k/k_s, k'_0 = k_0/k_s, q' = q/k_s \\ z' = \alpha \cos\gamma z_*, H' = \alpha \cos\gamma H_*, t' = \frac{\alpha \cos^2 \gamma k_s t}{\theta_s - \theta_r} \end{cases} \tag{8}$$

Next, the governing equation, the two boundary conditions and the initial condition for the rainfall infiltration into the monolithic cover can be rewritten as follows:

$$\begin{cases} \frac{\partial^2 k'}{\partial z'^2} + \frac{\partial k'}{\partial z'} = \frac{\partial k'}{\partial t'} \\ \frac{\partial k'}{\partial z'} + k' = q' \qquad z' = H' \\ \frac{\partial k'}{\partial z'} = 0 \qquad z' = 0 \\ k' = k'_0 \qquad t' = 0 \end{cases} \tag{9}$$

To solve Eq. (9), a transformation is defined as follows [19]:

$$k'(z', t') = W(z', t') e^{-\frac{1}{2}z' - \frac{1}{4}t'} \tag{10}$$

Next, Eq. (9) can be rewritten as:

$$\begin{cases} \frac{\partial^2 W}{\partial z'^2} = \frac{\partial W}{\partial t'} \\ \frac{\partial W}{\partial z'} + \frac{1}{2} W = q' e^{\frac{1}{2}z' + \frac{1}{4}t'} \qquad z' = H' \\ \frac{\partial W}{\partial z'} - \frac{1}{2} W = 0 \qquad z' = 0 \\ W = k'_0 e^{\frac{1}{2}z'} \qquad t' = 0 \end{cases} \tag{11}$$

The analytical solution for Eq. (11) can be obtained through the Fourier integral transform (a detailed solution is described in Appendix A) [19].

$$W(z', t') = \sum_{m=1}^{\infty} \frac{2[\beta_m \cos(\beta_m z') + 0.5 \sin(\beta_m z')]}{[(\beta_m^2 + 0.25)H' + 1](0.25 + \beta_m^2)} \left[\begin{array}{l} k'_0 \sin(\beta_m H')(0.25 + \beta_m^2) e^{\frac{1}{2}H' - \beta_m^2 t'} + \\ q' e^{\frac{1}{2}H'} [\beta_m \cos(\beta_m H') + 0.5 \sin(\beta_m H')] \\ \times (e^{\frac{1}{4}t'} - e^{-\beta_m^2 t'}) \end{array} \right] \tag{12}$$

The values of β_m are obtained as the positive roots of the following characteristic equation:

$$\tan(\beta_m H') = \frac{\beta_m}{\beta_m^2 - 0.25} \tag{13}$$

Using Eqs. (10) and (12), k' can be obtained as shown in Eq. (14):

$$k'(z', t') = \left\{ \begin{array}{l} \sum_{m=1}^{\infty} \frac{2[\beta_m \cos(\beta_m z') + 0.5 \sin(\beta_m z')]}{[(\beta_m^2 + 0.25)H' + 1](0.25 + \beta_m^2)} \times \\ \left[\begin{array}{l} k'_0 \sin(\beta_m H')(0.25 + \beta_m^2) e^{\frac{1}{2}H' - \beta_m^2 t'} + \\ q' e^{\frac{1}{2}H'} [\beta_m \cos(\beta_m H') + 0.5 \sin(\beta_m H')] \times \\ (e^{\frac{1}{4}t'} - e^{-\beta_m^2 t'}) \end{array} \right] \end{array} \right\} e^{-\frac{1}{2}z' - \frac{1}{4}t'} \tag{14}$$

Using Eqs. (2), (8) and (14), ψ can be obtained as

$$\psi = \frac{\ln\ k'}{\alpha} - \psi_{ae} \tag{15}$$

Using Eqs. (3) and (15), θ can be obtained as

$$\theta = \theta_r + (\theta_s - \theta_r) e^{\alpha(\psi + \psi_{ae})} \tag{16}$$

The percolation rate at the bottom boundary of the monolithic cover can be calculated using the following equation.

$$P_{er} = k' k_s \cos\gamma \tag{17}$$

It is well known that the percolation may continue for some time after the completion of the rainfall as a result of the delayed migration of rainwater. The analytical solution for calculating the percolation after the completion of the rainfall is shown in Eq. (18). The solution was derived in the same way as above but by replacing the q of Eq. (5) with 0 and the k_0 of Eq. (7) with k ($t = T$) obtained from Eq. (14); the subsequent solutions are the same as above. With Eq. (18), the rate of percolation after the completion of the rainfall can be calculated using Eq. (17).

$$k'(z', t'_2) = \left\{ \begin{array}{l} \sum_{m=1}^{\infty} \frac{2[\beta_m \cos(\beta_m z') + 0.5 \sin(\beta_m z')]}{[(\beta_m^2 + 0.25)H' + 1](0.25 + \beta_m^2)} e^{-\frac{1}{4}T' - \beta_m^2 t'_2} \times \\ \left[\begin{array}{l} k'_0 \sin(\beta_m H')(0.25 + \beta_m^2) e^{\frac{1}{2}H' - \beta_m^2 T'} + \\ q' e^{\frac{1}{2}H'} [\beta_m \cos(\beta_m H') + 0.5 \sin(\beta_m H')] \times \\ (e^{\frac{1}{4}T'} - e^{-\beta_m^2 T'}) \end{array} \right] \end{array} \right\} e^{-\frac{1}{2}z' - \frac{1}{4}t'_2} \tag{18}$$

where T is the duration of the entire rainfall process, t_2 is the time elapsed after the completion of the rainfall, and T' and t'_2 are the dimensionless parameters of T and t_2, respectively, where $T' = \frac{\alpha \cos^2 \gamma k_s T}{\theta_s - \theta_r}$ and $t'_2 = \frac{\alpha \cos^2 \gamma k_s t_2}{\theta_s - \theta_r}$.

3. Verification of the analytical solution

Numerical simulation was conducted to verify the analytical solution. The hydraulic properties of a silt soil reported by Aubertin et al. in 2009 [20], including the soil–water characteristic curve and the adapted hydraulic conductivity curve (Figs. 2 and 3), were used in the verification. The saturated volumetric water content and saturated hydraulic conductivity of the silt soil are 0.38 and 2×10^{-7} m/s, respectively. The data of hydraulic properties were fitted by using Eqs. (2) and (3), as shown in Figs. 2 and 3. The fitting parameters and other parameters are shown in Table 1. The numerical model of the monolithic cover used in the verification was established using the SEEP/W module of GEOSLOPE [12]. The thickness (H_*) of the model is set as 1 m, and the horizontal length is set to 30 m. The slope inclination of the model is set as 1:3. The upper boundary of the model is set as a constant flux boundary, which depends on rainfall intensity, and the lower boundary is set as the UG. The boundary conditions of the upstream and downstream regions of the model are all set as zero flux boundaries. The initial volumetric water content was assumed to be uniform and was set as the residual volumetric water content of the silt soil (i.e., 8%), corresponding to the initial unsaturated hydraulic conductivity set as 3.13×10^{-10} m/s [21]. It is assumed that the rainfall intensity is set as a constant value equivalent to two times

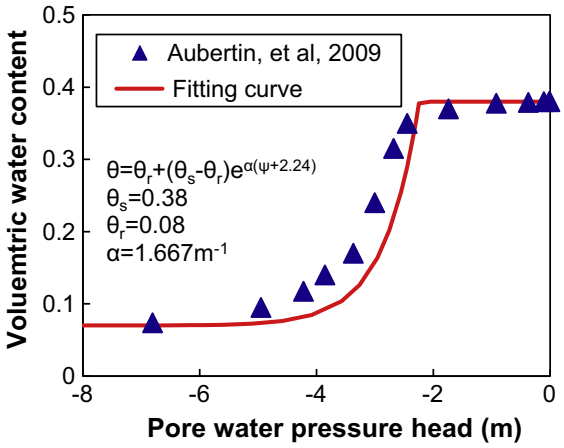

Fig. 2. Soil–water characteristic curve of the silt soil used in the verification.

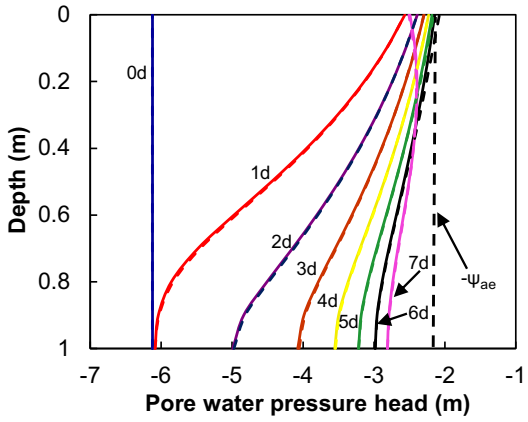

Fig. 4. Change in pore-water pressure head profile with time (solid lines: analytical result; dotted lines: numerical result).

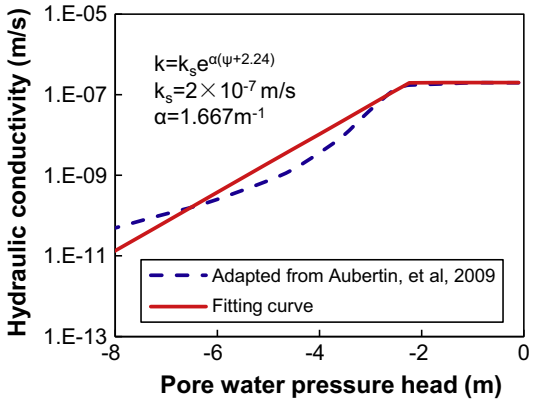

Fig. 3. Hydraulic conductivity curve of the silt soil used in the verification.

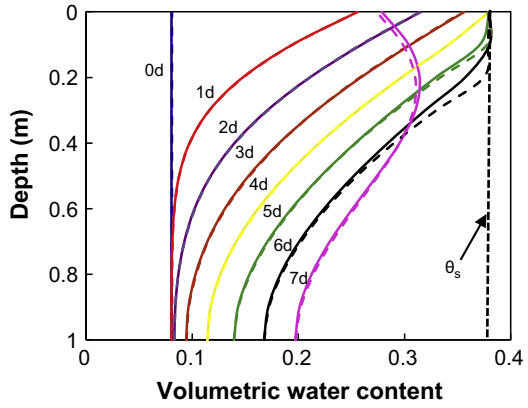

Fig. 5. Change in volumetric water content profile with time (solid lines: analytical result; dotted lines: numerical result).

the saturated hydraulic conductivity and lasts for 144 h (6 days). The applied rainfall intensity and duration are believed to be an extreme meteorological case for arid and semi-arid areas. After the completion of the rainfall, the duration of 24 h (1 day) is assumed for the delayed rainwater infiltration. Thus, the total duration of the rainwater infiltration into the monolithic cover is assumed to be 168 h (7 days).

Figs. 4 and 5 show the changes of pore water pressure profile and volumetric water content profile with time in the monolithic cover, respectively. As shown in Fig. 4, the pore water pressure profiles calculated by the analytical solution are very consistent with the numerical simulation when the duration of the rainfall is less than 5 days. On the 6th day, the analytical results deviate from the numerical results from the shallow soil, in which the pore water pressure increases to the negative air entry value ($-\psi_{ae}$), but the discrepancy is not significant. After completion of the rainfall, the pore water pressure profile calculated by the analytical solution is found to be consistent with the numerical simulation on the 7th day. Fig. 5 shows that the volumetric water content profiles calculated by the analytical solution are close to the numerical results, except that a slight difference exists on the 6th day, when the value of the pore water pressure at shallow soil is greater than that of the corresponding air entry value.

Fig. 6 shows the percolation rate calculated at the monolithic cover's bottom. It can be seen that the percolation rate calculated by the analytical solution is consistent with the numerical simulation result. The percolation starts to occur after 40 h of rainfall, and then the percolation rate continues to increase, even after the completion of the rainfall during the duration between 144 h and 168 h. The accumulated percolation for the entire process is 14.2 mm. These verification results indicate that the analytical solution can be used to calculate the deep percolation of the rainwater through the silty soil, which is commonly used as the material of a monolithic cover.

The numerical simulation was conducted again using the SF boundary (seepage face boundary) condition as the bottom boundary, and all the other parameters were the same as those used in

Table 1
Parameters used in the verification.

Horizontal length (m)	Vertical height H_* (m)	α (m^{-1})	ψ_{ae} (m)	θ_s	θ_r
30	1	1.67	2.2	0.38	0.08
Rainfall duration (h)	Duration of delayed rainwater infiltration (h)	k_s (m/s)	k_0 (m/s)	q (m/s)	H:V
144	24	2×10^{-7}	3.13×10^{-10}	4×10^{-7}	1:3

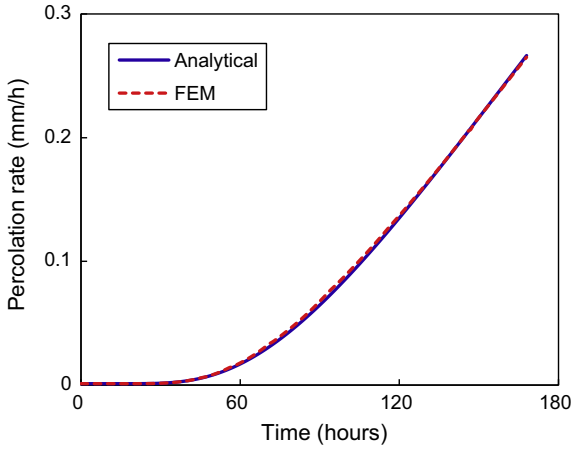

Fig. 6. Change in percolation rate with time.

the above numerical simulation. The numerical simulation results show that the accumulated percolation is 0 mm during the whole process because the SF boundary permits percolation to occur only when a saturated condition occurs at the bottom boundary. Thus, the UG boundary condition is more conservative than the SF boundary condition for the evaluation of deep percolation through a monolithic cover.

4. Analytical solutions for non-uniform rainfall infiltration into a monolithic cover

The intensity of a rainfall event in nature generally varied with time, exhibiting different patterns. Fig. 7 shows six representative rainfall patterns reported in the previous literatures [22,23]. These patterns consist of four basic rainfall types: uniform type (U), advanced type (A1 and A2), central-peaked type (C), and delayed type (D1 and D2). The advanced patterns have relatively high rainfall intensity during the early part of the rainfall event, whereas the delayed type peaked at the end of the rainfall event. The central-peaked pattern has a relatively high rainfall intensity in the middle part, whereas the uniform type has a constant rainfall intensity throughout the rainfall duration (T).

The expressions corresponding to the six different rainfall patterns are as follows:

$$\text{Expression of U pattern}: q(0 \leqslant t \leqslant T) \tag{19}$$

$$\text{Expression of A1 pattern}: \frac{q}{-T}(t-T) \quad (0 \leqslant t \leqslant T) \tag{20}$$

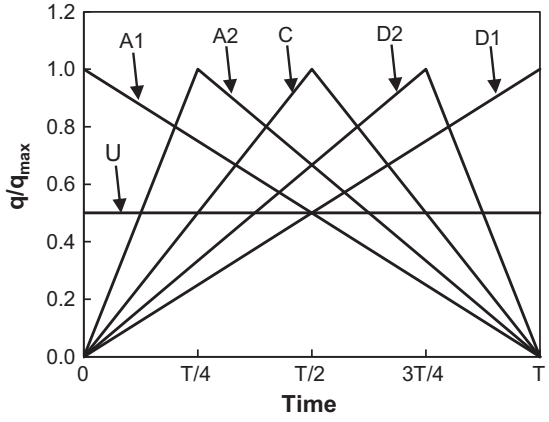

Fig. 7. Different patterns of rainfall lasting T hours [22,23].

$$\text{Expression of A2, C and D2 pattern}: \begin{cases} \frac{q}{T_1}t & (0 \leqslant t \leqslant T_1 0 \leqslant T_1 < T) \\ \frac{q}{T_1 - T}(t-T) & (T_1 \leqslant t \leqslant T 0 \leqslant T_1 < T) \end{cases} \tag{21}$$

$$\text{Expression of D1 pattern}: \frac{q}{T}t(0 \leqslant t \leqslant T) \tag{22}$$

where q is the peak rainfall intensity during the whole rainfall process; t is the time; T is the duration of the whole rainfall process; T_1 is the time of the rainfall increasing to its peak under the A2, C and D2 pattern.

When $0 < T_1 < T/2$, Eq. (21) expresses the A2 pattern (T_1 is set as $T/4$ in this article). When $T_1 = T/2$, Eq. (21) expresses the C pattern. When $T/2 < T_1 < T$, Eq. (21) expresses the D2 pattern (T_1 is set as $3T/4$ in the article).

The analytical solution corresponding to the U pattern was obtained in the second section of this paper. The analytical solution corresponding to the patterns A1 and D1 can be derived by replacing the q of Eq. (5) with the expressions (20) and (22), respectively; the subsequent solutions are the same as above. For the patterns A2, C and D2, the solution consists of two parts. For the first part, when $0 \leqslant t \leqslant T_1$, the solution is the same as above. For the second part, when $T_1 < t \leqslant T$, the k_0 of Eq. (7) must be replaced by $k\,(t = T_1)$, which can be solved in the first part. The unified form of an analytical solution for the six different rainfall patterns is given by Eq. (23), and the solution is shown in Appendix A.

$$k'(z',t') = \left\{ \begin{array}{l} \sum_{m=1}^{\infty} \frac{2[\beta_m \cos(\beta_m z') + 0.5\sin(\beta_m z')]}{\left[\left(\beta_m^2 + 0.25\right)H' + 1\right]\left(0.25 + \beta_m^2\right)} \times \\ \left[k_0' \sin(\beta_m H')\left(0.25 + \beta_m^2\right) e^{\frac{1}{2}H' - \beta_m^2 t'} \times D_i + \right. \\ \left. q' e^{\frac{1}{2}H'} [\beta_m \cos(\beta_m H') + 0.5\sin(\beta_m H')] \times E_i \right] \end{array} \right\} e^{-\frac{1}{2}z' - \frac{1}{4}t'} \tag{23}$$

where D_i and E_i are coefficients corresponding to the six different patterns, as shown in Table 2. In Table 2, T_1' and T' are, respectively, the dimensionless parameters of T_1 and T, where $T_1' = \frac{\alpha \cos^2 \gamma k_s T_1}{\theta_s - \theta_r}$, $T' = \frac{\alpha \cos^2 \gamma k_s T}{\theta_s - \theta_r}$. Note: for the A2, C and D2 patterns, the t' in Eq. (23) is equal to $t' - T_1'$, when $T_1 < t \leqslant T$.

The analytical solution for calculating the percolation rate after the completion of the rainfall with the U pattern is obtained in the second section of this paper. The analytical solutions corresponding to the other patterns can be derived as shown in Eq. (24) by replacing the q of Eq. (5) with 0 and the k_0 of Eq. (7) with the k ($t = T$) obtained from Eq. (23).

$$k'(z',t_2') = \left\{ \begin{array}{l} \sum_{m=1}^{\infty} \frac{2[\beta_m \cos(\beta_m z') + 0.5\sin(\beta_m z')]}{\left[\left(\beta_m^2 + 0.25\right)H' + 1\right]\left(0.25 + \beta_m^2\right)} e^{-\beta_m^2 t_2' - \frac{1}{4}T'} \times \\ \left[k_0' \sin(\beta_m H')\left(0.25 + \beta_m^2\right) e^{\frac{1}{2}H' - \beta_m^2 T'} \times F_i + \right. \\ \left. q' e^{\frac{1}{2}H'} [\beta_m \cos(\beta_m H') + 0.5\sin(\beta_m H')] \times G_i \right] \end{array} \right\} e^{-\frac{1}{2}z' - \frac{1}{4}t_2'} \tag{24}$$

Table 2
Expressions for E_i and D_i in Eq. (23) corresponding to the six different patterns.

Type		D_i	E_i
U		1	$e^{\frac{1}{2}t'} - e^{-\beta_m^2 t'}$
A1		1	$\frac{1}{T'}\left(t' e^{0.25t'} - \frac{e^{0.25t'} - e^{-\beta_m^2 t'}}{0.25 + \beta_m^2}\right) - e^{0.25t'} + e^{-\beta_m^2 t'}$
A2, C and D2	$0 \leqslant t' \leqslant T_1'$	1	$\frac{1}{T_1'}\left[t' e^{0.25t'} - \frac{e^{0.25t'} - e^{-\beta_m^2 t'}}{(0.25 + \beta_m^2)}\right]$
	$T_1' < t' \leqslant T'$	$e^{-(0.25+\beta_m^2)T_1'}$	$e^{-\beta_m^2 t'} - \frac{e^{-\beta_m^2 t'}[1 - e^{-(0.25+\beta_m^2)T_1'}]}{T_1'(\beta_m^2 + 0.25)} + \frac{\left[t' e^{0.25t'} - \frac{e^{0.25t'} - e^{-\beta_m^2 t'}}{\beta_m^2 + 0.25}\right]}{T_1' - T'} + [e^{0.25t'} - e^{-\beta_m^2 t'}]$
D1		1	$\frac{1}{T'}\left(t' e^{0.25t'} - \frac{e^{0.25t'} - e^{-\beta_m^2 t'}}{0.25 + \beta_m^2}\right)$

where F_i and G_i are coefficients corresponding to the six different patterns, as shown in Table 3. Note: for the A2, C and D2 patterns, the T' in the Eq. (24) is equal to $T' - T'_1$, and the T' of $T'_1 - T'$ in Table 3 must remain constant.

Eqs. (23) and (24) were used to investigate the influence of the six rainfall patterns on the volumetric water content profiles and the percolation rate through the monolithic cover, and the delayed rainwater infiltration through the monolithic cover after the completion of the rainfall. It is assumed that the total rainfall is kept the same, and the rainfall intensity of the pattern U and the peak rainfall intensity of the other five patterns are 2 and 4 times that of the soil's saturated hydraulic conductivity, respectively. The other parameters are the same as that used by the above analytical model for verification. The calculated volumetric water content profiles at various times for the six rainfall patterns are shown in Fig. 8. For all six rainfall patterns, the volumetric water contents at the different depths of the monolithic cover all increase gradually during the first 3 days. In addition, for the pattern A1, the volumetric water contents increase the most rapidly because its rainfall intensity is the greatest during the first 3 days, followed by the patterns A2, C, U, D2 and D1. In contrast, during the period between 4 and 6 days, the increasing trend of the volumetric water content is different between the six rainfall patterns. As shown in Fig. 8, the volumetric water contents for the pattern D1 increase the most rapidly because its rainfall intensity during the later period is the greatest, followed by the patterns D2, U, C, A2 and A1. During the later period, the volumetric water contents at the shallow depth for the patterns A1, A2 and C even gradually decrease because the amount of rainfall infiltration becomes less than the water migrating from the shallow soil into the deep soil layer. After the completion of the rainfalls, the profiles of volumetric water content for the six rainfall patterns can be calculated using Eq. (24), as shown in Fig. 8. Over the 7 days, the volumetric water content in the deep soil layer for the pattern A1 is the largest, and followed by the patterns A2, C, U, D2 and D1, whereas the volumetric water content in the shallow soil layer is just the opposite. Because the total rainfall is the same for all six patterns, the more rainfall there is during the first half of the rainfall period, the greater the amount of water migrating from the shallow soil layer into the deep soil layer. The greater the rainfall is during the second half of the period, the more water there is that will be stored in the shallow soil layer.

Fig. 9 shows the calculated percolation of rainwater through the monolithic cover for the six patterns of rainfall. The percolation for the pattern A1 is found to occur the earliest. This result corresponds to the most rapid increase in volumetric water content at the bottom of the monolithic cover for the pattern A1. After the percolation occurs, the percolation rate for the pattern A1 is always highest during the whole process of the 168 h, followed by the patterns A2, U, C, D2 and D1, with the exception that the percolation rate for the pattern C is greater than that for the pattern U after the completion of rainfall (i.e., during the period between 144 h and 168 h). Fig. 9 shows that the accumulated value of percolation at 168 h for the patterns A1, A2, U, C, D2 and D1 is 20.9 mm, 16.6 mm, 14 mm, 12.7 mm, 9.49 mm and 7.26 mm, respectively. The accumulated value of percolation is proportional to the accumulated value of rainfall during the first half of the rain period because the rainwater requires a period of time to migrate from the shallow soil layer into the deep soil layer and to percolate. Because the total rainfall is kept the same for all the six patterns, the greater the intensity of the rainfall is during the first half of the period, the greater the percolation at the bottom. The greater the rainfall intensity is during the second half of the rain period, the larger the amount of rain water stored in the soil is. Note that the accumulated rainfall for the patterns U and C is identical during the first half of the period. However, the accumulated percolation of the pattern U is greater than that for pattern C because more rainfall occurs later during the first half of the rain period for the pattern C compared with the pattern U.

Table 3
Expressions for F_i and G_i in Eq. (24), corresponding to the six different patterns.

Type	F_i	G_i
U	1	$e^{\frac{1}{4}T'} - e^{-\beta_m^2 T'}$
A1	1	$\frac{1}{T'}\left(T' e^{0.25T'} - \frac{e^{0.25T'} - e^{-\beta_m^2 T'}}{0.25+\beta_m^2}\right) - e^{0.25T'} + e^{-\beta_m^2 T'}$
A2, C and D2	$e^{-(0.25+\beta_m^2)T'_1}$	$e^{-\beta_m^2 T'} - \frac{e^{-\beta_m^2 T'}\left[1-e^{-(0.25+\beta_m^2)T'_1}\right]}{T'_1(\beta_m^2+0.25)} + \frac{\left[T' e^{0.25T'} - \frac{e^{0.25T'} - e^{-\beta_m^2 T'}}{\beta_m^2+0.25}\right]}{T'_1 - T'} + [e^{0.25T'} - e^{-\beta_m^2 T'}]$
D1	1	$\frac{1}{T'}\left(T' e^{0.25T'} - \frac{e^{0.25T'} - e^{-\beta_m^2 T'}}{0.25+\beta_m^2}\right)$

5. Practical application

The above analytical solution (i.e., Eqs. (23) and (24)) can be used to predict the percolation of rainwater through a monolithic cover subjected to different patterns of rainfall event. Fig. 10 shows a flow chart for the prediction. At the first step, all the rainfall events within the considered period (e.g., a representative wet season) must be identified according to the meteorological data. At the second step, the initial water storage (S_0) in the monolithic cover prior to each rainfall event (q) should be estimated. The estimated S_0 is required to determine the initial condition for the analytical solution (Eq. (23)), as well as to identify the rainfall event that will result in percolation. Estimation is performed by following the antecedent rainfall method proposed by Crozier and Eyles in 1980 [24]. The method was meant to estimate the antecedent rainfall (q_a) prior to a specific rainfall event (q) for the analysis of a rain-induced slope failure. The antecedent rainfall (q_a) is calculated by Eq. (25), in which a 10-day period prior to the rainfall event (q) is considered.

$$q_a = Kq_1 + K^2 q_2 + \cdots K^n q_n \tag{25}$$

where q_n is the daily rainfall on the nth day prior to the considered rainfall event (q). The maximum value of n was adopted 10 by Crozier and Eyles [24]. This value can be a different value when required. K is an empirical parameter.

The estimated antecedent rainfall (q_a) is somewhat a measurement of the water storage in the shallow soil layer. It is assumed that Eq. (26) can be used to quantify the initial water storage (S_0) in the monolithic cover prior to the rainfall event (q).

$$S_0 = c + q_a \tag{26}$$

where c is another empirical parameter. The two empirical parameters (K and c) depend on the meteorological characteristic and the hydrological response of monolithic cover, and they can be calibrated by the data monitoring water balance. This calibration will be demonstrated in the case study presented later.

With the estimated initial water storage (S_0), the initial condition for the analytical solution (Eq. (23)) can be determined by assuming the water content is uniformly distributed along the depth of the monolithic cover. The uniform value of the initial water content (θ_0) prior to the rain event (q) is equal to the initial water storage (S_0) divided by the cover thickness (L) (i.e., $\theta_0 = S_0/L$).

At the third step, with the estimated initial water storage (S_0) prior to each rainfall event, the rainfall events that tend to produce percolation can be screened from all of the rainfall events. The screening is performed by comparing the sum of initial water storage (S_0) and the rainfall quantity of the considered event (q) with the water storage capacity (S_f) of the monolithic cover. If the sum

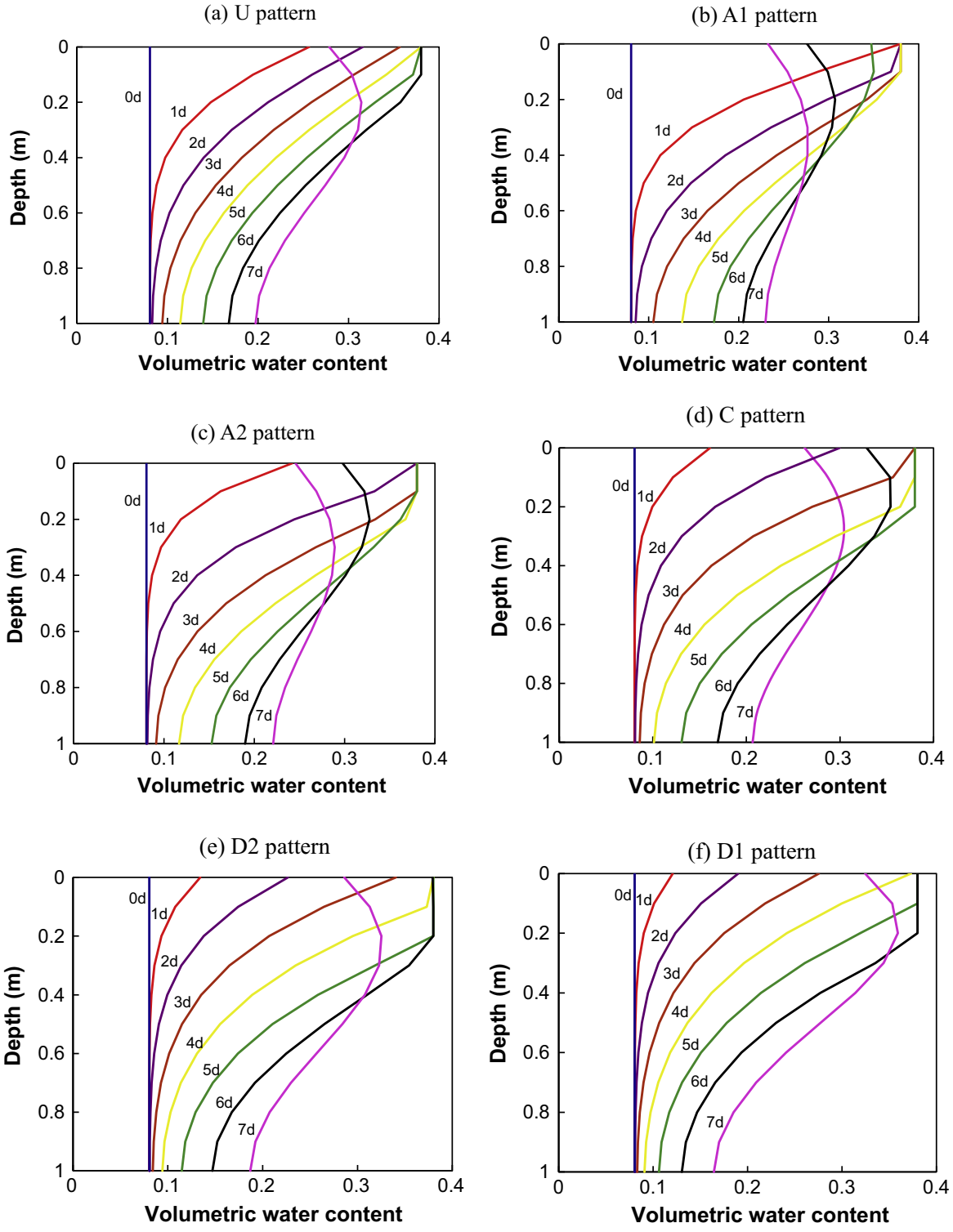

Fig. 8. Changes in volumetric water content profile with time for the six rainfall patterns.

is greater than the storage capacity, percolation tends to occur, and the considered rainfall event will be identified. The theoretical water storage capacity (S_f) of the monolithic cover is equal to the field capacity of the soil (θ_c) multiplied by the cover thickness (L) [25].

In the fourth step, the rainfall pattern and duration of the identified events should be determined in accordance with the availability of meteorological data. If the meteorological data is provided on an hourly basis, then one of the expressions for the six rainfall patterns (Eqs. (19)–(22)) can be used to fit the hourly rainfall data, and the duration can also be obtained. If the meteorological data are provided on a daily basis, then the rainfall pattern must be estimated according to the description of the weather record and the experience on the seasonal rainfall characteristics. For example, in the summer (June to August) of Wuhan City in China, a heavy rainfall (greater than 50 mm/d) often occurs within

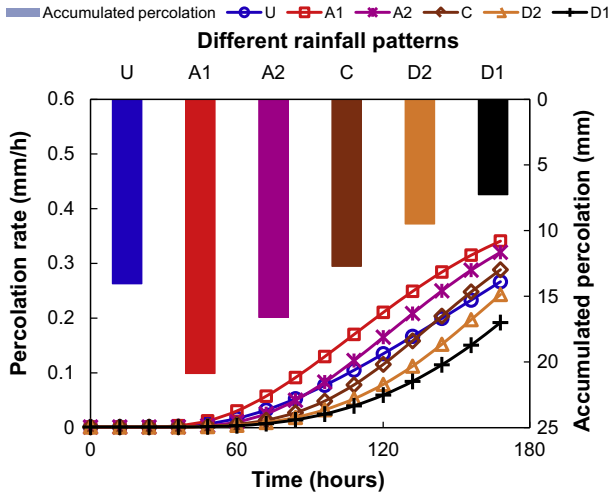

Fig. 9. Percolation rate and accumulated percolation for the six patterns of rainfall.

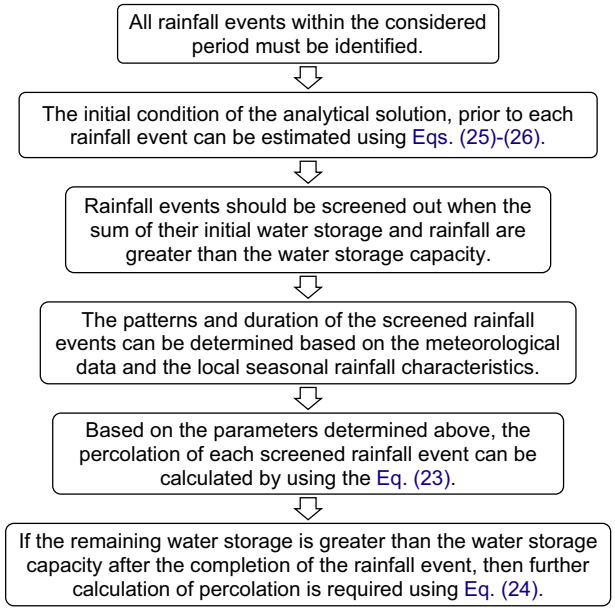

Fig. 10. Flow chart for predicting percolation through a monolithic cover.

12 h, and the intensity firstly increases to a peak and then decreases to 0 [26]. Thus, the rainfall can be assumed to follow pattern C within 12 h.

At the fifth step, with the initial condition, the rainfall pattern and duration for each of the identified rainfall events, the percolation of rainwater through the monolithic cover within the duration of the rainfall event can be calculated by using Eq. (23). Finally, the percolation may continue after completion of the rainfall event. Thus, the remaining water storage in the cover at the end of the rainfall event should be checked against the water storage capacity (S_f) of the monolithic cover. If the remaining water storage is greater than the water storage capacity (S_f), then further calculation of percolation is required using Eq. (24). This calculation should be performed until the remaining water storage is less than the water storage capacity (S_f).

The following describes a case study performed to demonstrate how to use the above analytical solutions (Eqs. (23) and (24)) to predict percolation through a monolithic cover, based on the model test result reported by Liu et al. in 2009 [27]. The model test was performed to investigate the performance of a monolithic cover during the wet seasons in Wuhan China. The model box, placed horizontally, was 3.6 m long, 1.3 m wide and 1.3 m high. A MSW waste layer with a thickness of 0.6 m was placed at the bottom of the model box. The monolithic cover, consisting of a silty soil layer (0.6 m in thickness) planted with shrubs, was placed on the waste layer. TDR probes were installed at three depths (0.2 m, 0.4 m and 0.6 m) in the soil cover to measure the distribution of water content, so that the water storage within the soil cover could be deduced. Three funnel-shaped collection devices were installed at the bottom of the monolithic cover to measure percolation. The daily rainfall was measured by the weather station nearby. The model test allowed for surface ponding when the rainfall intensity was greater than the infiltration ability, i.e., all rainwater infiltrated into the monolithic cover during the test.

The hydraulic properties of the cover soil used for the model test reported by Liu et al. [27] are shown in Figs. 11 and 12. The saturated volumetric water content and saturated hydraulic conductivity for the soil were 0.44 and 8.1×10^{-6} m/s, respectively. The soil–water characteristic curve and hydraulic conductivity curve were fitted by using Eqs. (2) and (3). The two fitting curves and parameters are shown in Figs. 11 and 12.

The distribution of daily rainfall during the model test period (May 16, 2007 to December 10, 2007) is shown in Fig. 13; the accumulated rainfall was 696.3 mm. The measurements of water storage and daily percolation through the soil cover during the period are also shown in Fig. 13. The initial water storage (S_0) for each of the rainfall events can be calculated using Eqs. (25) and (26). The empirical parameters c and K were back analyzed as 0.96 and 80, respectively. The back analysis was based on the measurements of water storage prior to each of the rainfall events. The water storage capacity (S_f) was estimated as 210 mm, according to the data of water storage recorded prior to the observed percolation (see Fig. 13).

Four rainfall events, corresponding to May 30, June 29, June 30 and July 3, were identified as being able to produce percolation because the sum of the initial water storage (S_0) and the current rainfall depth (q) was greater than the water storage capacity (S_f = 210 mm). The values of the initial water storages (S_0) prior to the three rainfall events of May 30, June 29, June 30 and July 3 were calculated as 129.7 mm, 186 mm, 196 mm and 193.7 mm, respectively, as shown in Table 4. The daily rainfall on May 30 was 115 mm (heavy rain) and was assumed to be distributed within the first 12 h, with the C pattern according to the local experience of rainfall characteristics in the period [26]. The percolation through the soil cover during the rainfall period of 12 h was calculated as 5.9 mm by using Eq. (23). The remaining water storage (S_0) at the completion of the rainfall event was calculated as 238.8 mm, which was greater than the water storage capacity (S_f = 210 mm);

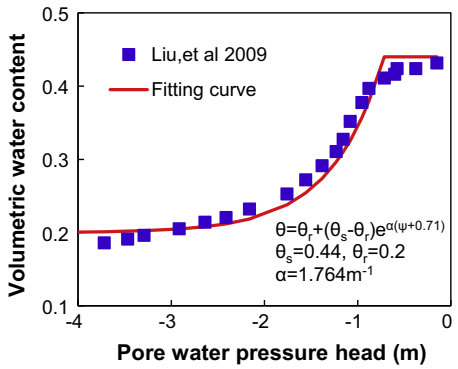

Fig. 11. Soil–water characteristic curve for the cover soil.

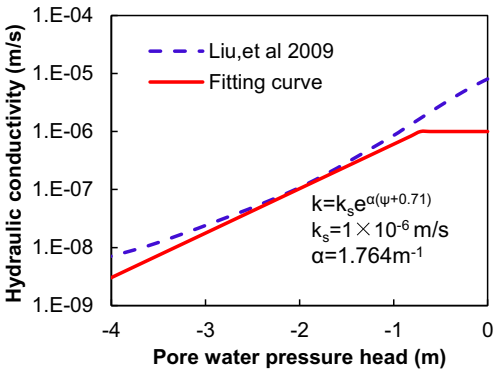

Fig. 12. Hydraulic conductivity curve for the cover soil.

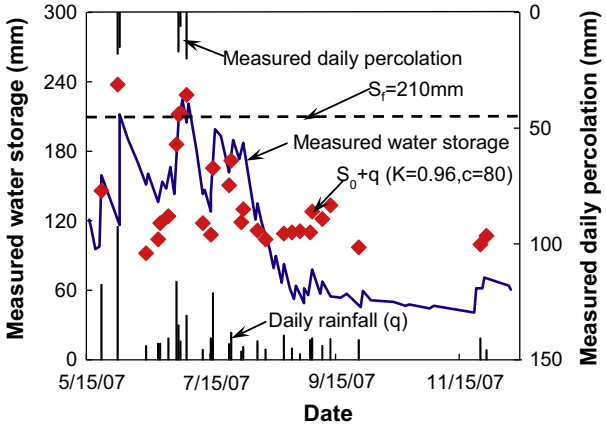

Fig. 13. Measured water storage, daily percolation and precipitation.

thus, further calculation of percolation was conducted by using Eq. (24). The further percolation lasting 24 h was calculated as 29.8 mm. As a result, the total percolation for the rainfall event on May 30 was calculated as 35.7 mm, which is close to the measurement (33 mm). The daily rainfall on June 29, June 30 and July 3 was 30 mm, 16 mm and 39 mm, respectively. The rainfall for all three events was assumed to distribute within the first 12 h with the U pattern, according to the local experience of rainfall characteristics at the period. The predicted values of percolation for the three rainfall events (June 29, June 30 and July 3) were 20 mm, 22.3 mm and 23.8 mm, which were greater than the measurements (i.e., 17 mm, 6 mm and 20 mm).

A comparison between the predicted percolation and the measurements is shown in Table 4. It can be seen that the proposed analytical method can capture all the percolation events observed during the test period, and the predicted total percolation was 101.8 mm, 34% greater the measured result of 76 mm. The comparison indicated that the prediction of percolation through a monolithic cover by using the analytical method is on the conservative side.

Table 4
Comparison of the predicted daily percolation and the measured result.

Rainfall event	Rainfall (mm)	Initial water storage (S_0) (mm)	$S_0 + q$ (mm)	Percolation (mm)	
				Predicted result	Measured result
May 30	115	129.7	$244.7 > S_f$	35.7	33
June 29	30	186	$216 > S_f$	20	17
June 30	16	196	$212 > S_f$	22.3	6
July 3	39	193.7	$232.7 > S_f$	23.8	20
Accumulated percolation				101.8	76

6. Conclusions and suggestions

This paper presented an analytical solution for evaluating the infiltration and deep percolation of rainwater into a monolithic cover, subject to different patterns of rainfall events, including uniform type (U), advanced type (A1 and A2), central-peaked type (C), and delayed type (D1 and D2). The analytical solution is derived from the simplified one-dimensional governing equation of unsaturated flow for an infinite long monolithic cover by taking the exponential forms of the soil–water characteristic curve and the hydraulic conductivity curve into account. A comparison between the analytical solution and the numerical simulation demonstrated that the analytical solution is acceptable for the silty soil, which is commonly used as the material for a monolithic cover. The analytical solution was further applied to evaluate the total percolation of a monolithic cover being subjected to a sequence of non-continuous rainfall events within a wet season. The evaluation accounted for the influence of initial water storage in the cover on the percolation by using the antecedent rainfall method proposed by Crozier and Eyles in 1980. A case study was performed to demonstrate the evaluation approach based on the water balance monitoring data of a model test on a silty soil cover reported in the literature. The case study indicated that the prediction of percolation from the analytical solution is 34% greater than the measurement, being on the conservative side for practical application. The analyses of the six rainfall patterns indicated that the greater the rainfall intensity during the first half of rainfall period is, the earlier the deep percolation occurs, and the accumulated percolation increased with the rainfall depth during the first half period. The analytical solution provides a simple and potential tool for evaluating the hydrological performance of a monolithic cover. For practical application of the analytical solution, further work is required with respect to the calibration of the model parameters with detailed meteorological data and an accumulation of water balance monitoring data for monolithic covers.

Acknowledgements

The authors acknowledge the financial support from the National Basic Research Program of China (973 Program) (2012CB719805) provided by the National Natural Science Foundation of China (NSFC).

Appendix A

W can be obtained from

$$W = \sum_{m=1}^{\infty} \frac{X}{N} e^{-\beta_m^2 t'} [F + A]$$

in which X, N, A and F are given by

$$\begin{cases} X = \beta_m \cos(\beta_m z') + 0.5 \sin(\beta_m z') \\ N = 0.5\left[(\beta_m^2 + 0.25)H' + 1\right] \end{cases}$$

$$A = \begin{cases} e^{\frac{1}{2}H'} X(z' = H') \int_0^{t'} e^{(\beta_m^2 + 0.25)t^*} Q dt^* & \text{U, A1, D1 pattern with } 0 \leqslant t \leqslant T \\ e^{\frac{1}{2}H'} X(z' = H') \int_0^{t'} e^{(\beta_m^2 + 0.25)t^*} Q dt^* & \text{A2, C, D2 pattern with } 0 \leqslant t \leqslant T_1, 0 \leqslant T_1 \leqslant T \\ e^{\frac{1}{2}H'} X(z' = H') \int_0^{t'} e^{(\beta_m^2 + 0.25)(t^* - T_1')} Q dt^* & \text{A2, C, D2 pattern with } T_1 \leqslant t \leqslant T, 0 \leqslant T_1 \leqslant T \end{cases}$$

$$F=\begin{cases} k'_0\int_0^{H'} e^{\frac{1}{2}z'}Xdz' & \text{U, A1, D1 pattern, and A2, C, D2 pattern with } 0\leqslant t\leqslant T_1 \\ \int_0^{H'}\sum_{m=1}^{\infty}\frac{X}{N}e^{-\beta_m^2 T'_1}\left[k'_0\int_0^{H'} e^{\frac{1}{2}z'}Xdz' + e^{\frac{1}{2}H'}q'X(z'=H')\int_0^{T'_1} e^{(\beta_m^2+0.25)t^*}\frac{t^*}{T'_1}dt^*\right] & \text{A2, C, D2 pattern with } T_1\leqslant t\leqslant T \end{cases}$$

with

$$Q=\begin{cases} q' & \text{U pattern} \\ \frac{q'(t^*-T')}{-T'} & \text{A1 pattern} \\ \frac{q't^*}{T'_1} & \text{A2, C, D2 pattern}(0\leqslant t\leqslant T_1, 0\leqslant T_1\leqslant T) \\ \frac{q'(t^*-T')}{(T'_1-T')} & \text{A2, C, D2 pattern}(T_1\leqslant t\leqslant T, 0\leqslant T_1\leqslant T) \\ \frac{q't^*}{T'} & \text{D1 pattern} \end{cases}$$

References

[1] Albright WH, Gee GW, Wilson GV, Fayer MJ. Alternative cover assessment project: phase I report, Publication No. 41183. Desert Research Institute; 2002.
[2] Hauser VL, Weand BL, Gill MD. Natural covers for landfills and buried waste. J Environ Eng 2001;127(9):768–75.
[3] Schnabel W, Lee W, Barnes DL. A numerical simulation of evapotranspiration landfill cover performance at three cold-region locations. In: World Water and Environmental Resources Congress. Anchorage, Alaska. p. 1–8 [in United States].
[4] Sun JL, Yuen STS, Fourie AB. The effect of using a geotextile in a monolithic (evapotranspiration) alternative landfill cover on the resulting water balance. Waste Manage 2010;30:2074–83.
[5] Bohnhoff GL, Ogorzalek AS, Benson CH, Shackelford CD, Apiwantragoon P. Field data and water-balance predictions for a monolithic cover in a semiarid climate. J Geotech Geoenviron Eng 2009;135(3):333–48.
[6] Albright WH, Benson CH, Gee GW, Roesler AC, Abichou T, Apiwantragoon P, et al. Field water balance of landfill final covers. J Environ Qual 2004;33(6):2317–32.
[7] Scanlon BR, Reedy RC, Keese KE, Dwyer SF. Evaluation of evapotranspirative covers for waste containment in arid and semiarid regions in the southwestern USA. Vadose Zone J 2005;4(1):55–71.
[8] McGuire PE, Andraski BJ, Archibald RE. Case study of a full-scale evapotranspiration cover. J Geotech Geoenviron Eng 2009;135(3):316–32.
[9] Benson CH, Bohnhoff GL, Ogorzalek AS, Shackelford CD, Apiwantragoon P, Albright WH. Field data and model predictions for a monolithic alternative cover. In: Geo-Frontiers Congress. Austin, Texas. p. 1–16 [in United States].
[10] Khire MV, Benson CH, Bosscher PJ. Water balance modeling of earthen final covers. J Geotech Geoenviron Eng 1997;123(8):744–54.
[11] Zhang WJ, Qiu ZH, Zhou CR, Peng GL. Evaluation of evapotranspiration covers of landfills in Yangtze River delta region. Chin J Geotech Eng 2009;31(3):384–9.
[12] Zhan TLT, Jia GW, Chen YM, Fredlund DG, Li H. An analytical solution for rainfall infiltration into an unsaturated infinite slope and its application to slope stability analysis. Int J Numer Anal Meth Geomech 2013;37(12):1737–60.
[13] Zhan LT, Jia GW, Chen YM, Fredlund DG. Analytical solution for rainfall infiltration into infinite long slopes considering properties of unsaturated soil. Chin J Geotech Eng 2010;32(8):1214–20.
[14] Srivastava R, Yeh TCJ. Analytical solutions for one-dimensional, transient infiltration toward the water table in homogeneous and layered soils. Water Resour Res 1991;27(5):753–62.
[15] Huang RQ, Wu LZ. Analytical solutions to 1-D horizontal and vertical water infiltration in saturated/unsaturated soils considering time-varying rainfall. Comput Geotech 2012;39:66–72.
[16] Wu LZ, Zhang LM. Analytical solution to 1D coupled water infiltration and deformation in unsaturated soils. Int J Numer Anal Meth Geomech 2009;33(6):773–90.
[17] Wu LZ, Zhang LM, Huang RQ. Analytical solution to 1D coupled water infiltration and deformation in two-layer unsaturated soils. Int J Numer Anal Meth Geomech 2012;36(6):798–816.
[18] Fredlund MD. SoilVision Systems Ltd. SVFlux User's Manual. Saskatoon, Saskatchewan, Canada; 2009.
[19] Ozisik MN. Boundary value problems of heat conduction. New York: Dover; 1989.
[20] Aubertin M, Cifuentes E, Apithy SA, Bussiere B, Molson J, Chapuis RP. Analyses of water diversion along inclined covers with capillary barrier effects. Can Geotech J 2009;46(10):1146–64.
[21] Khire MV, Benson CH, Bosscher PJ. Capillary barriers: design variables and water balance. J Geotech Geoenviron Eng 2000;126(8):695–708.
[22] Ng CWW, Wang B, Tung YK. Three-dimensional numerical investigations of groundwater responses in an unsaturated slope subjected to various rainfall patterns. Can Geotech J 2001;38(5):1049–62.
[23] Tsai TL. The influence of rainstorm pattern on shallow landslide. Environ Geol 2008;53(7):1563–9.
[24] Crozier MJ, Eyles RJ. Assessing the probability of rapid mass movement. In: Third Australia–New Zealand Conference on Geomechanics [in Wellington].
[25] Chen C. Meteorological Conditions for Design of Monolithic Alternative Earthen Covers (AEFCs), MS Thesis. Madison, Wisconsin, USA: University of Wisconsin; 1999.
[26] Mao YW. The analysis and forecasting research of short-duration rainstorm in Wuhan MS Thesis. Lanzhou, China: Lanzhou University; 2013.
[27] Liu CS, Zhao H, Luo JW. Experiment and numerical simulation of percolation control using evapotranspirative landfill cover system. Environ Sci 2009;30(1):289–96 [in Chinese].